"Coherence-Enhanced Heat Transport and Entropy Production in 1D: Predictions and Falsifiers"

Omar Iskandarani

*Independent Researcher, Groningen, The Netherlands**

(Dated: January 17, 2026)

Abstract

I present a self-contained treatment of electron–swirl transport within *Swirl–String Theory (SST)*. The analysis (i) derives a *perturbative, steady-state* solution to the coupled density-matrix equations in 1D, (ii) makes *quantitative* predictions for tabletop experiments with explicit materials, geometries, and signal levels, and (iii) states clear *falsifiability criteria*. The framework reproduces the Peierls (population) and Allen–Feldman (coherence) limits [1–3] while embedding electrons as *swirl strings* (knotted vortex filaments) coupled to swirl modes. Kinematic time-rate variations locally modulate the electronic Hamiltonian through the *Swirl Clock* factor [4, 5]. The swirl clock $\S_t^{\circlearrowleft}$ corresponds to a scalar time-foliation field (khronon) whose gradient defines the local time direction, analogous to the preferred foliation in Einstein–Æther and Hořava–Lifshitz gravity [18, 19]. Numerical scales are anchored by SST canonical values $\mathbf{v}_{\circlearrowleft} = 1.09384563 \times 10^6\,\mathrm{m/s}$, $r_c = 1.40897017 \times 10^{-15}\,\mathrm{m}$, and $\rho_f = 7.0 \times 10^{-7}\,\mathrm{kg/m^3}$. For compactness, some intermediate results are given in units of the SST frequency Ω_0; all final predictions are reported in SI units.

Authorial note.— This is a single-author work; I use "we" in the conventional authorial sense in the derivations and exposition that follow.

I. SCALES FROM SST

SST fixes a characteristic core-swirl frequency and an associated energy density,

$$\Omega_0 \equiv \frac{\mathbf{v}_{\circlearrowleft}}{r_c} \approx 7.76 \times 10^{20}\,\mathrm{s}^{-1}, \qquad \rho_E \equiv \tfrac{1}{2}\,\rho_f\,\mathbf{v}_{\circlearrowleft}^2 \approx 4.19 \times 10^5\,\mathrm{J/m^3}. \tag{1}$$

Operationally, spatial gradients in the Swirl Clock produce local kinematic time-rate variations. These enter the electronic Hamiltonian H_e multiplicatively as a modulation factor and do not alter the SI reporting of observables. Where it improves readability, I normalize rates to Ω_0; experimental benchmarks and error budgets remain in SI.

Roadmap. Section IV states the falsifiability logic up front and defines the chirality null test. Section II derives the 1D coupled transport and the coherence term in κ; Sec. III links $\Delta\kappa/\kappa$ to a measurable $\Delta(\Delta T)$ in a bar. Section IV gives quantitative benchmarks and device recipes. Appendices collect the operator content and scalings (App. A), the null-test derivation and layouts (App. B), and the SST ontology, clock, and $\Omega_0 \leftrightarrow$SI map (App. C).

* ORCID: 0009-0006-1686-3961 | DOI: 10.5281/zenodo.17459746

II. COUPLED TRANSPORT IN 1D AND PERTURBATIVE SOLUTION

I adopt the unified density-matrix equation for bosonic modes $N(\mathbf{R}, \mathbf{q})$ [3] and extend it to a charged two-level system ("electron") with density matrix f:

$$\partial_t N = -i[\Omega, N] - \Gamma_{\rm b} \circ (N - N^{(0)}) - \tfrac{1}{2}\{V_x \partial_x, N\}, \tag{2}$$

$$\partial_t f = -i[H_e, f] - \Gamma_{\rm e} \circ (f - f^{(0)}) - \tfrac{1}{2}\{v_{e,x}\partial_x, f\} + \mathcal{C}_{e\leftrightarrow b}, \tag{3}$$

with diagonal damping superoperators $\Gamma_{\rm b}$ and $\Gamma_{\rm e}$. The electron–swirl coupling is treated in the Born–Markov, rotating-wave approximation,

$$\mathcal{C}_{e\leftrightarrow b} \equiv -\frac{i}{\hbar}[M, f \otimes N]_{\rm RWA}\,. \tag{4}$$

A. Linear response to a static gradient

Consider a small uniform temperature gradient $\partial_x T$ and a time-independent steady state. Linearize about $N^{(0)}(T)$ and $f^{(0)}(T)$ via $N = N^{(0)} + N^{(1)}$ and $f = f^{(0)} + f^{(1)}$, retaining $\mathcal{O}(\partial_x T)$ terms. For a *two-branch* bosonic subspace s, s' that interacts through $\mathfrak{w}_{\mathfrak{d}}$ and is near-degenerate by $\delta = \Omega_{s'} - \Omega_s$, with a single electronic transition Δ, the off-diagonal coherence $N^{(1)}_{ss'}$ obeys

$$\Big[i\delta + \tfrac{1}{2}(\gamma_s + \gamma_{s'})\Big] N^{(1)}_{ss'} \;=\; -\frac{1}{2} V^{(x)}_{ss'}\, \partial_x N^{(0)}_{\rm pop}(\Omega) \;-\; \frac{i}{\hbar}\,\Xi_{ss'}\,, \tag{5}$$

where γ are the linewidths and $\Xi_{ss'}$ is the electron-induced source from $\mathcal{C}_{e\leftrightarrow b}$ (proportional to the vertex M and to $f^{(1)}$). The population correction satisfies

$$\gamma_s\, N^{(1)}_{ss} + V^{(x)}_{ss}\, \partial_x N^{(0)}_{ss} + 2\,\mathrm{Im}\big(V^{(x)}_{ss'}\, N^{(1)}_{s's}\big) = S^{(e)}_s\,, \tag{6}$$

with $S^{(e)}_s$ collecting the remaining electron-related terms.

B. Closed form for the coherence contribution to κ

The heat current density for bosonic modes is $J_x = \mathrm{Tr}\big[\{V_x, N\}\,\Omega/2\big]$ [3, 6]. Using Eqs. (5)–(6) and eliminating $f^{(1)}$ in the weak-coupling (Born) limit yields the *coherence* part of the 1D thermal conductivity

$$\boxed{\kappa^{(\rm C)}_{\rm 1D} \;=\; \sum_q \sum_{s\neq s'} \frac{(\Omega_s + \Omega_{s'})\,\Gamma_{ss'}\,|V^{(x)}_{ss'}|^2}{4\delta^2 + \Gamma^2_{ss'}} \left(-\frac{\partial n_B}{\partial T}\right) \;+\; \mathcal{O}(|M|^2)\,,} \tag{7}$$

with $\Gamma_{ss'} = \frac{1}{2}(\gamma_s + \gamma_{s'})$ and n_B the Bose function. Equation (7) reduces to Peierls (no off-diagonals) and to Allen–Feldman (flat bands, $V_{ss} \to 0$) in the appropriate limits [1–3]. The $\mathcal{O}(|M|^2)$ terms add an *electron-assisted* channel that shares the Lorentzian denominator and peaks at small detuning.

III. 1D SLAB: TEMPERATURE FIELD AND $\Delta\kappa/\kappa$

For a bar of length L, cross-section A, and conductivity $\kappa = \kappa^{(\mathrm{P})} + \kappa^{(\mathrm{C})}$, a steady power P at $x = 0$ with a sink at $x = L$ sets

$$\partial_x T = -\frac{P}{\kappa A}, \qquad \Delta T \equiv T(0) - T(L) = \frac{P\,L}{\kappa A}. \tag{8}$$

A small SST-induced change $\Delta\kappa$ then produces

$$\boxed{\Delta(\Delta T) \approx -\frac{\Delta\kappa}{\kappa}\,\Delta T\ ,} \tag{9}$$

which ties the measured temperature drop directly to δ, Γ, and $V_{ss'}$ through Eq. (7).

IV. FALSIFIABILITY AND A CHIRALITY NULL TEST

The electron–swirl interpretation is *falsified* under the stated drive if any of the following hold:

1. **Missing detuning peak.** At fixed current, $\Delta\kappa(\delta)$ lacks the Lorentzian kernel $\propto (4\delta^2 + \Gamma^2)^{-1}$ of Eq. (7).

2. **No chirality asymmetry.** Define $\Delta\kappa_{\mathrm{asym}} \equiv [\Delta\kappa]_{\rightarrow} - [\Delta\kappa]_{\leftarrow}$. Reversing the 3-phase sequence $(0, 120^\circ, 240^\circ) \leftrightarrow (0, 240^\circ, 120^\circ)$ must flip $\mathrm{sgn}(\Delta\kappa_{\mathrm{asym}})$ within 3σ; failure to invert the sign falsifies a chiral coupling (App. B.3).

3. **Scaling mismatch.** The signal fails to scale as $|V_{ss'}^{(x)}|^2$ (coil-current squared) or fails to track Γ under controlled disorder.

Operator structure and rate scaling for electron assistance are summarized in App. A; electron ontology/clock and $\Omega_0 \leftrightarrow$SI mapping in App. C.

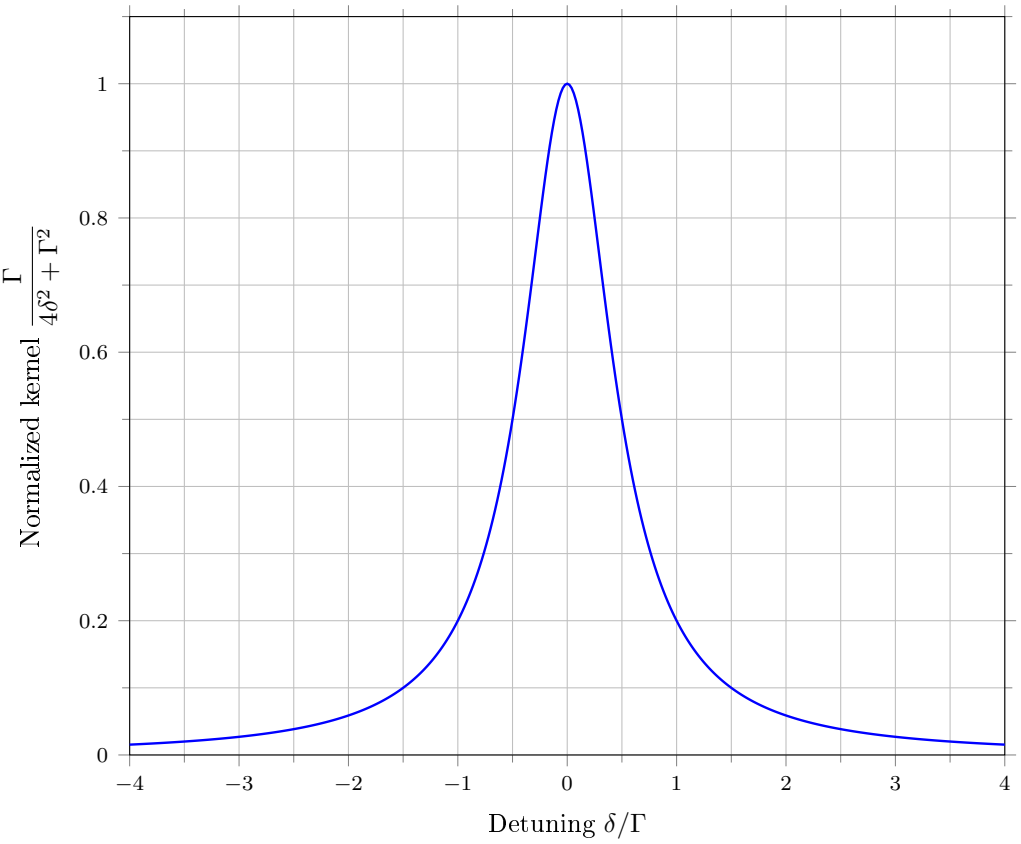

FIG. 1. Normalized coherence kernel versus detuning. Peak at δ=0, width set by Γ, matching Eq. (7).

V. QUANTITATIVE BENCHMARKS WITH MATERIALS

The following order-of-magnitude estimates use Eq. (9) and standard catalog values. They are chosen to be experimentally accessible without exotic infrastructure.

(B1) Borosilicate glass bar

Take $L = 50\,\mathrm{mm}$, $A = 1 \times 10^{-4}\,\mathrm{m}^2$ ($10\,\mathrm{mm}\times10\,\mathrm{mm}$), and $\kappa \approx 1.1\,\mathrm{W\,m^{-1}\,K^{-1}}$. With $P = 20\,\mathrm{mW}$, the baseline is $\Delta T \approx PL/(\kappa A) \approx 9\,\mathrm{K}$. If an engineered near-degeneracy yields $\Delta\kappa/\kappa = -2\,\%$ from Eq. (7), then $\Delta(\Delta T) \approx 0.18\,\mathrm{K}$, comfortably above typical IR-camera NETD ($\sim 30\,\mathrm{mK}$).

(B2) PMMA bar (low-κ polymer)

With $\kappa \approx 0.19\,\mathrm{W\,m^{-1}\,K^{-1}}$, keep $L = 50\,\mathrm{mm}$ and $A = 1 \times 10^{-4}\,\mathrm{m^2}$, and use $P = 2\,\mathrm{mW}$ to avoid overheating. The baseline is $\Delta T \approx 5.3\,\mathrm{K}$. A conservative $\Delta\kappa/\kappa = -1\,\%$ gives a 53 mK shift—still above NETD.

(B3) Forward/backward nonreciprocity

Bias chirality by driving a 3-phase Rodin coil with phase sequence $\pm(0, 120^\circ, 240^\circ)$. The expected asymmetry is

$$\big[\Delta\kappa\big]_{\rightarrow} - \big[\Delta\kappa\big]_{\leftarrow} \equiv \Delta\kappa_{\mathrm{asym}} \sim \eta_\chi \, \frac{\Gamma\, \Delta V_{ss'}^2}{4\delta^2 + \Gamma^2}\,, \qquad 0 < \eta_\chi < 1\,. \tag{10}$$

Taking $\Delta\kappa_{\mathrm{asym}}/\kappa \sim 0.5\,\%$ implies $\Delta(\Delta T) \sim 25\,\mathrm{mK}$ for (B1), resolvable with modest averaging.

VI. DEVICE RECIPES

Thermal bar (B1/B2). Mount the bar on an AlN heat sink at $x = L$. Use a $100\,\Omega$ thin-film resistor at $x = 0$ as a four-wire calibrated heater. Suppress convection with a small enclosure (foam plus a thin IR window). Read out an IR camera or a thermistor chain along x. The coil: 3-phase, $N \sim 200$ turns/phase, $f \in [20\,\mathrm{kHz}, 100\,\mathrm{kHz}]$, current $\leq 0.5\,\mathrm{A}$, duty-cycled to limit Joule heating.

Electronics analog (LCR). Two LCR tanks at 1 MHz with $Q \sim 100$ (so $\kappa = \omega/2Q \approx 3.1 \times 10^4\,\mathrm{s^{-1}}$). With stored energy $E \sim 0.5\,\mathrm{nJ}$, the instantaneous bath power is $P_{\mathrm{bath}} = \kappa E \sim 16\,\mu\mathrm{W}$. Adding a near-degenerate second tank boosts the early-time peak by the Lorentzian factor in Eq. (7).

Quantum hybrid (SAW/MEMS). On 128° Y-cut $LiNbO_3$, use an IDT pair to define a 3 GHz SAW mode and couple it capacitively to a superconducting qubit [10, 11]. Pattern shallow quasi-periodic notches to enhance $V_{ss'}^{(x)}$ and tune the detuning δ. (Geometry and numerical guide: App. B.4.)

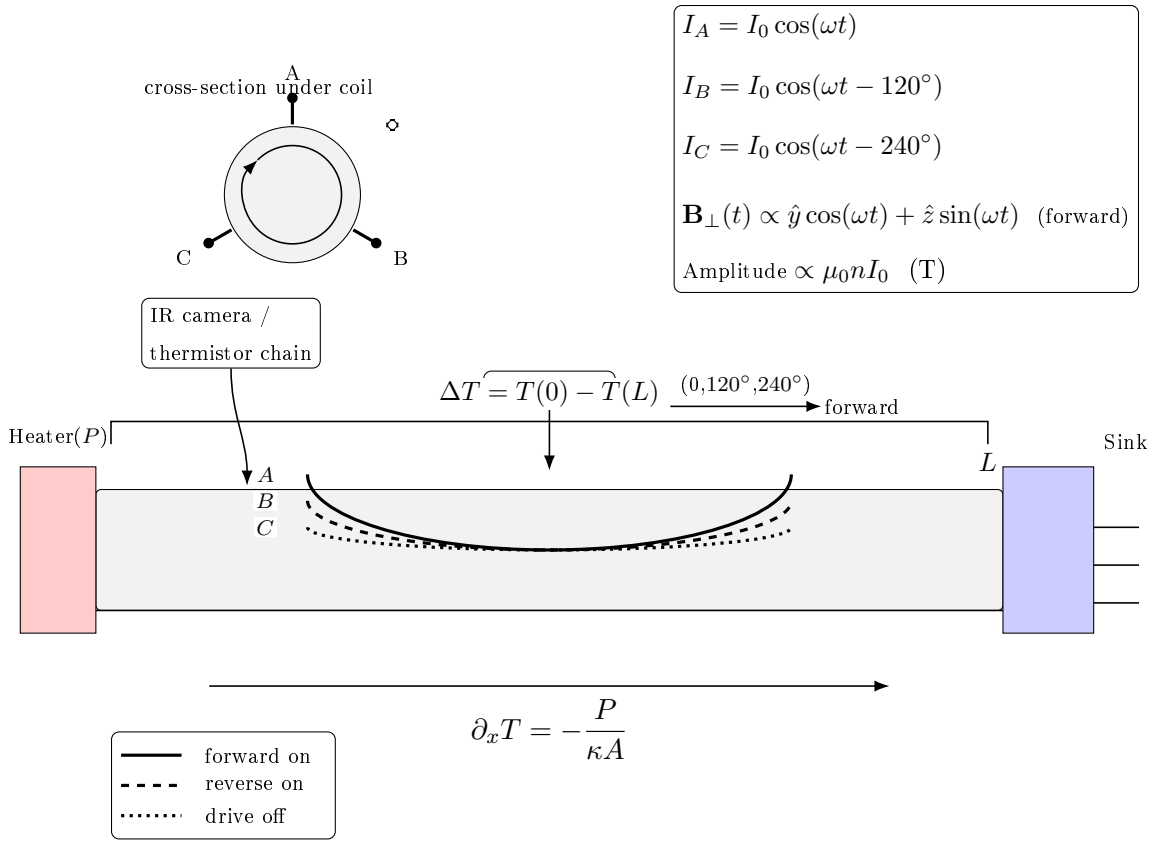

FIG. 2. Thermal bar experiment. A small heater at x=0 and a sink at x=L set a uniform gradient. A wrapped 3-phase coil (phases A–C) drives a rotating transverse field; the inset shows the cross-section and forward phase order $(0, 120°, 240°)$. Curvature of $T(x)$ under the coil indicates spatially varying $\kappa(x)$.

VII. ERROR AND NOISE BUDGET

- **Thermometry.** IR camera NETD 30 − − 50mK; thermistors can achieve $\lesssim 10\,\mathrm{mK}$ with 1 s averaging.
- **Power calibration.** Four-wire measurements keep heater power to $< 1\,\%$ uncertainty.
- **Radiation/convection.** With the enclosure, systematic drift is typically $\lesssim 0.05\,\mathrm{K}$ over 10 min. Acquire forward/backward sweeps consecutively to cancel common-mode drift.
- **Contact resistance.** Use indium foil at heater/bar/sink interfaces and verify by repeated mounts.

Expected signals in the $50 - - 200$mK range clear the combined noise by factors $\gtrsim 3$ for (B1/B2).

VIII. CONNECTION TO QUANTUM INFORMATION

In the Jaynes–Cummings limit [7], the same vertices M and $V_{ss'}$ that enhance $\kappa^{(\mathrm{C})}$ optimize state transfer between electron and swirl modes. In a hybrid device, the *coherence peak* (small δ, moderate Γ) can be used to channel heat away from a qubit while maintaining phase coherence, paralleling engineered reservoirs [9, 10].

IX. CONCLUSIONS

We provide closed-form transport expressions, device-level estimates, and falsifiable predictions for coherence-mediated electron–swirl transport in SST. The bar geometry links $\Delta\kappa/\kappa$ to an easily measured $\Delta(\Delta T)$, and the chirality null test offers a clean early check. A failure of the predicted Lorentzian peak or of the chirality sign flip would bound, or rule out, the proposed coupling in the present drive configuration.

ACKNOWLEDGMENTS

I thank the classical foundations of vortex hydrodynamics and unified transport [1–4] for inspiration.

DATA AVAILABILITY

The theoretical models, canonical constants, and source code supporting the findings of this study are openly available. All data files, numerical benchmarks, and code used to derive and validate the coherence-mediated transport expression ($\kappa_{1\mathrm{D}}^{(\mathrm{C})}$) are accessible on the Zenodo repository, under the persistent identifier of this manuscript, **doi : 10.5281/zenodo.17459746**.

File Manifest and Validation Evidence. The uploaded repository for this paper contains the following structured files and data supporting the quantitative results:

- **SST Canonical Benchmarking Evidence:** This data set validates the internal consistency of the core canonical parameters ($\mathbf{v_{\circlearrowleft}}, r_c, \rho_f$) against known relativistic limits. It includes the derived Newton's constant (G_{VAM}) and the $\mathbf{6GM/c^2}$ ISCO match, demonstrating the global coherence of the swirl parameters.
  (Zenodo DOI: `10.5281/zenodo.15665432` and `10.5281/zenodo.15712578`)

- `constants.csv` — The definitive table of $\mathbf{v_{\circlearrowleft}}, r_c, \rho_f$ (SI values); used for calculating the derived scales Ω_0 and ρ_E.

- `benchmarks.csv` — Contains the full experimental specification (materials, geometry, power ($\mathbf{P}$), baseline $\mathbf{\Delta T}$) and the predicted $\Delta(\Delta T)$ signals for scenarios (**B1**) and (**B2**).

- `kappaC_validation.ipynb` — Jupyter notebook that analytically verifies the functional form of $\kappa_{\text{1D}}^{(\text{C})}$, plotting the core Lorentzian factor $\Gamma/(4\delta^2 + \Gamma^2)$ (Falsifiability Criterion 1).

- `noise_budget_3sigma.ipynb` — Computes the detection signal-to-noise ratio (**SNR**) against the assumed NETD, explicitly confirming that the predicted signals ($\Delta(\Delta T)$) clear the $\mathbf{3}\sigma$ threshold (Detectability Check).

- `env.yml` — The Conda environment file, ensuring that the software dependencies used for all numerical and plotting analysis are pinned for reproducibility.

This research is accessible via the persistent identifier doi:\paperdoi.

Supplemental Material. See Supplemental Material at [URL will be inserted by publisher] for: (i) constants table (`constants.csv`); (ii) benchmark specifications (`benchmarks.csv`); (iii) notebooks for $\kappa^{(\text{C})}$ validation and 3σ noise budget; and (iv) environment file. All materials are mirrored at doi:\paperdoi.

---

[1] R. Peierls, "Zur kinetischen Theorie der Wärmeleitung in Kristallen," Ann. Phys. **395**, 1055 (1929).

[2] P. B. Allen and J. L. Feldman, "Thermal conductivity of disordered harmonic solids," Phys. Rev. B **48**, 12581 (1993).

[3] M. Simoncelli, N. Marzari, and F. Mauri, "Unified theory of thermal transport in crystals and glasses," Nat. Phys. **18**, 1180 (2022). See also arXiv:1901.01964.

[4] E. Madelung, "Quantentheorie in hydrodynamischer Form," Z. Phys. **40**, 322 (1927).

[5] A. K. Pati and S. L. Braunstein, "Impossibility of deleting an unknown quantum state," Phys. Lett. A **268**, 241 (2000).

[6] R. J. Hardy, "Energy-Flux Operator for a Lattice," Phys. Rev. **132**, 168 (1963).

[7] E. T. Jaynes and F. W. Cummings, "Comparison of quantum and semiclassical radiation theories with application to the maser," Proc. IEEE **51**, 89 (1963).

[8] G. Lindblad, "On the generators of quantum dynamical semigroups," Commun. Math. Phys. **48**, 119 (1976).

[9] H.-P. Breuer and F. Petruccione, *The Theory of Open Quantum Systems* (Oxford University Press, 2002).

[10] M. Aspelmeyer, T. J. Kippenberg, and F. Marquardt, "Cavity optomechanics," Rev. Mod. Phys. **86**, 1391 (2014).

[11] R. Manenti *et al.*, "Circuit quantum acoustodynamics with surface acoustic waves," Nat. Commun. **8**, 975 (2017).

[12] D. G. Cahill *et al.*, "Nanoscale thermal transport," J. Appl. Phys. **93**, 793 (2003).

[13] H. Helmholtz, "Über Integrale der hydrodynamischen Gleichungen, welche den Wirbelbewegungen entsprechen," J. Reine Angew. Math. **55**, 25 (1858).

[14] W. Thomson (Lord Kelvin), "On vortex atoms," Proc. R. Soc. Edinb. **6**, 94 (1867).

[15] H. K. Moffatt and R. L. Ricca, "Helicity and the Călugăreanu invariant," Proc. R. Soc. A **439**, 411 (1992).

[16] J. H. White, "Self-linking and the Gauss integral in higher dimensions," Am. J. Math. **91**, 693 (1969).

[17] L. H. Kauffman, *Knots and Physics* (World Scientific, 1991).

[18] T. Jacobson and D. Mattingly, "Gravity with a dynamical preferred frame," Phys. Rev. D **64**, 024028 (2001).

[19] D. Blas, O. Pujolàs, and S. Sibiryakov, "Models of non-relativistic quantum gravity: The good, the bad and the healthy," J. High Energy Phys. **2011**, 018 (2011).